Effects of Slope and Aspect Variations on Satellite Surface Temperature Retrievals and Mesoscale Analysis in Mountainous Terrain

ALAN E. LIPTON

Atmospheric Sciences Division, Geophysics Directorate, Phillips Laboratory, Hanscom Air Force Base, Massachusetts

(Manuscript received 11 March 1991, in final form 28 July 1991)

ABSTRACT

Surface temperature retrieval in mountainous areas is complicated by the high variability of temperatures that can occur within a single satellite field of view. Temperatures depend in part on slope orientation relative to the sun, which can vary radically over very short distances. The surface temperature detected by a satellite is biased toward the temperatures of the sub-field-of-view terrain elements that most directly face the satellite. Numerical simulations were conducted to estimate the effects of satellite viewing geometry on surface temperature retrievals for a section of central Colorado. Surface temperatures were computed using a mesoscale model with a parameterization of subgrid variations in slope and aspect angles.

The simulations indicate that the slope–aspect effect can lead to local surface temperature variations up to 30°C for autumn conditions in the Colorado mountains. For realistic satellite viewing conditions, these variations can give rise to biases in retrieved surface temperatures of about 3°C. Relative biases between retrievals from two satellites with different viewing angles can be over 6°C, which could lead to confusion when merging datasets. The bias computations were limited by the resolution of the available terrain height data (~90 m). The results suggest that the biases would be significantly larger if the data resolution was fine enough to represent every detail of the real Colorado terrain or if retrievals were made in mountain areas that have a larger proportion of steep slopes than the Colorado Rockies. The computed bias gradients across the Colorado domain were not large enough to significantly alter the forcing of the diurnal upslope–downslope circulations, according to simulations in which surface temperature retrievals with view-dependent biases were assimilated into time-continuous analyses. View-dependent retrieval biases may be relevant to climatological analyses that rely on remotely sensed data, given that bias-induced errors are systematic.

1. Introduction

Ground surface temperatures are a critical factor in surface energy fluxes by way of their effects on sensible, latent, and radiative energy transfer. It is therefore necessary to estimate surface temperatures when studying atmospheric processes, such as mesoscale circulations, that depend heavily on surface fluxes. Short-range forecasts and climatological analyses can be particularly reliant on surface temperature estimation.

Direct measurements of surface temperature are difficult to make and are generally not available with sufficient coverage or resolution for mesoscale applications. Indirect measurements can be made using satellite-based infrared sounders, which give broad coverage and high spatial and temporal resolution. The primary drawback of this method is that the accuracy of surface temperature retrievals is sensitive to cloud cover, and they cannot be made at all under overcast conditions. Errors in the assumed surface emittance can be another significant source of retrieval error, as several researchers have pointed out. Emittance-related errors up to about 1.5°C can be expected for retrievals over land with 11-μm data (Kornfield and Susskind 1977; Sutherland 1986). Nevertheless, satellite-retrieved surface temperatures can be very useful for mesoscale analysis when cloud cover is incomplete. For example, Lipton and Vonder Haar (1990b) used 3-h retrievals from the VISSR Atmospheric Sounder (VAS) in a four-dimensional numerical analysis of circulations in the mountains and plains of the northeastern Colorado region. In this type of analysis, the surface temperature retrieval process is coupled with numerical modeling.

Surface temperature retrieval in mountainous areas is complicated by the high variability of temperatures that can occur within a single field of view of the satellite sounder or a single grid box of the analysis domain—on the order of 10 km. Primary factors in temperature variability are terrain elevation, ground cover, soil characteristics, and slope orientation relative to the sun. The orientation (slope and aspect) factor is particularly relevant to satellite retrievals because it relates directly to the satellite's viewing geometry and it can vary radically within a satellite field of view.

The immediate effect of surface orientation is to reg-

Corresponding author address: Dr. Alan E. Lipton, PL/GPAS, Hanscom Air Force Base, MA 01731-5000.

ulate the insolation at the ground (Geiger 1965), but the ultimate effect on surface temperatures depends heavily on vegetative cover and soil characteristics, with the effect being greater for sparser vegetation and drier soil (Sader 1986; Avissar and Pielke 1989). Large effects appear to be possible, although most observational data are somewhat ambiguous. Astling and Quattrochi's (1989) remotely sensed data included an elevation-corrected difference of ~23°C between a pair of shaded and illuminated slopes in Utah. Whiteman et al. (1989a) reported surface temperature differences of up to 16°C between east- and west-facing slopes of moderate steepness (36° and 42°) in September in the Colorado mountains.

The surface temperature detected by a satellite is biased toward the temperatures of the sub–field-of-view terrain elements that most directly face the satellite. As an illustration, we can consider a satellite field of view divided into N discrete terrain elements of equal size, where the value of N is arbitrary. Figure 1 is an example of a divided terrain region that could be part of (or contain) a field of view. The average surface radiance in the direction of the satellite is

$$L_s = \frac{\sum_{i=1}^{N} B_\lambda(T_i)\epsilon_i \cos\gamma_i}{\sum_{i=1}^{N} \cos\gamma_i}, \qquad (1)$$

where $B_\lambda(T_i)$ is the blackbody radiance at wavelength λ of an element at temperature T_i, ϵ_i is the surface emittance, and γ_i is the angle between the satellite's view and the normal to a terrain element. The equivalent average temperature could be computed as $T_s = B_\lambda^{-1}(L_s)$.

We can isolate the effects of viewing geometry and simplify the equation by assuming that $\epsilon_i = 1$ and that the relationship between blackbody radiance and temperature is linear over the range of temperatures in the field of view. These assumptions, and their significance, are addressed later in this section and in section 4c, respectively. With these assumptions, the effective surface temperature in the direction of the satellite is

$$T_s = \frac{\sum_{i=1}^{N} T_i \cos\gamma_i}{\sum_{i=1}^{N} \cos\gamma_i}. \qquad (2)$$

Here T_s would differ most greatly from an unweighted average of T_i when there is a strong correlation between the cosines and the temperatures. This could occur, for example, when the satellite and the sun are aligned and at a large angle from the local zenith.

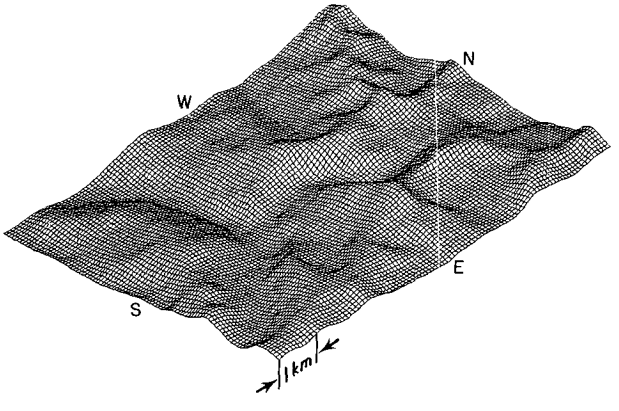

FIG. 1. A diagram of terrain elevations at 3″ resolution for a 5′ × 5′ region in Colorado. The area covered is the southwest quarter of the model grid box centered at 39°25′N, 106°30′W (denoted with an arrow in Fig. 3). The viewing perspective is from the location of a geostationary satellite at longitude 75°W.

Differences between satellite-view–weighted average temperatures and unweighted average temperatures represent a component of surface temperature error when satellite retrievals are used in meteorological analysis—the effects of viewing geometry directly reduce the degree to which retrieved surface temperatures are representative of the true energy fluxes. This error component must be zero when γ is constant throughout the field of view, so error gradients may be present in an analysis when terrain is smooth in one part of a domain and irregular in another part. Such error gradients were not considered in the mountain–plains analysis of Lipton and Vonder Haar (1990b).

The assumption that $\epsilon_i = 1$ is not as restrictive as it might appear at first glance. Surface emittances can vary significantly within the area covered by a field of view (Sutherland 1986; Van de Griend et al. 1991), but they would be relevant to the effect of satellite viewing geometry only if they were correlated with the viewing-angle cosines. Such correlations could occur (e.g., when some slopes are more vegetated than others) but would generally be weak and difficult to quantify.

Numerical simulations were conducted to estimate the effects of satellite viewing geometry on surface temperature retrievals for realistic mountain topography. Surface temperatures for a region in Colorado were computed using a mesoscale model with a surface energy balance algorithm. The resolution of the topography in the model experiments was varied from 10′ to 3″ lat/long to determine the effect of resolution on the viewing geometry effect. Satellite-apparent temperatures could then be computed for various satellite viewing angles and times of day and compared with true (unweighted average) temperatures. Finally, an evaluation was made of the errors' impact on simulated mesoscale circulations when satellite-view temperatures were assimilated into a numerical time-continuous analysis.

2. Modeling methodology

A version of the Colorado State University Regional Atmospheric Modeling System (CSU RAMS) was used

for the simulations. The model formulation is hydrostatic and incompressible, with a terrain-following grid and parameterizations for stable and convective boundary layers (Mahrer and Pielke 1977, 1978; McNider and Pielke 1981). Soil temperatures are determined by computing surface fluxes and subsurface heat diffusion. The radiation parameterization takes account of slope and aspect angles when computing insolation at the surface. Radiative flux estimates are input to the surface energy balance algorithm, which can be invoked to compute surface temperatures.

Ideally, a simulation of surface temperatures over irregular terrain would have model resolution at least as fine as the terrain data resolution so that the microscale effects of ridges and valleys could be explicitly treated. A prohibitive amount of computer power would be needed to deal with 3″ (~90 m) resolution. Instead, the model was run at 10′ (~18 km) resolution and the features of subgrid terrain elements were parameterized, as was suggested by Avissar and Pielke (1989).

Each subgrid terrain element was classified according to its slope and aspect angles. There were 41 classes, as illustrated in Fig. 2, where the range of possible slope angles was divided into 10° bands and each band was divided into equal-sized segments of aspect angle. The number of segments per band was specified such that each slope–aspect class would cover roughly the same amount of solid angle. Each class was then separated into two parts—directly illuminated elements and elements shaded by nearby terrain—yielding 82 classes. The model's treatment of radiation was modified so that shaded elements received only diffuse radiation (see the Appendix). During its integration, the model accessed tabulated data for each grid box indicating how many subgrid elements belonged to each class. For each class that was occupied by at least one element, a separate energy balance computation was made to solve for the surface temperature. The energy balance computations included separate surface-layer parameters and soil profile temperatures for each class. The grid-average surface temperature was then computed as the average of the temperatures for each class, weighted by the number of elements in the class. The surface-layer parameterization was reinvoked, this time at the grid scale, to compute surface fluxes consistent with the grid-average temperature. These grid-representative fluxes were used in the grid-scale dynamic equations.

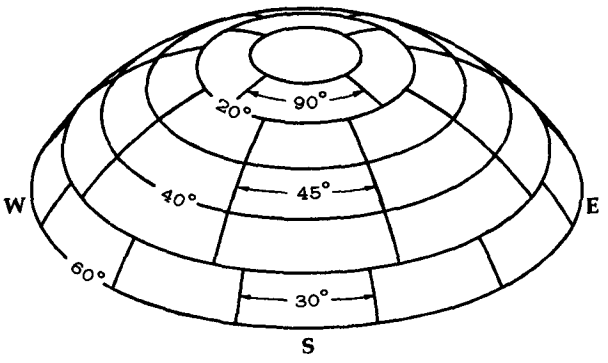

FIG. 2. An illustration of the classification boundaries for slope and aspect angles. There are six bands of slope angle, each 10° wide. The lengths of aspect-angle divisions are as labeled. The letters at the perimeter denote the directions.

The class assignment of each terrain element was permanent with regard to slope/aspect, but the sunlit–shaded assignment changed as the solar position changed during the simulation period. The presence or absence of shading was computed for every element using an algorithm that determined whether a terrain element was obstructed by any neighboring element along a particular line of sight (such as the sun's). This method accounts for elements facing entirely away from the line of sight as well as elements facing toward the line of sight but obstructed by a nearby hill or mountain. Obstructions were searched for within a range of up to 100 element lengths (~9 km, for 3″ data) along the ground projection of the view path. The range was limited due to computer time constraints and, for the Colorado data, could have resulted in sunrise–sunset time errors up to 40 min. Such errors could occur only when the sun was very low in the sky, and they appeared to be rare. Obstructions were found by computing the altitude of each terrain-element edge along the view path projection and comparing it with the altitude of the view path. At 5-min intervals, a computer program tabulated the number of sunlit and shaded elements in each slope–aspect class for each model grid box.

This parameterization of terrain orientation effects can vastly reduce the number of energy balance computations needed per grid point per time step—from 40 000 to ≤82 when applied to 3″ data on a 10′ grid. One weakness of the method is that the classifications do not fully take account of differences in the *histories* of shading at different elements, which affect the storage and release of heat in the soil. For example, any two sunlit elements facing west at 25° inclination will be assigned the same temperature even if one just emerged from a shadow and the other has been illuminated for 2 h. The energy budget computations for a given sunlit class were initialized when the first member of that class became illuminated, where the initial soil profile temperatures were taken from the corresponding shaded class. Similarly, the computations for each shaded class were initialized when the first class member became shaded, using sunlit initialization data. The impact of this characteristic of the parameterization was determined by making model runs in which separate energy budgets were computed for the median and last members of each class to change illumination. The worst surface temperature error due to neglecting

shading history was 4°C and the errors were typically less than 0.5°C.

In all of the computations, we assumed that there were no differences in ground cover, albedo, soil moisture, or deep soil temperature according to slope or aspect angles. Such differences occur commonly in semiarid climates such as Colorado's, where slopes that receive less solar radiation on an annual basis have cooler, moister soil and denser vegetation (Whiteman et al. 1989b; Blackwell et al. 1980). In some cases, these factors may represent a positive feedback, in which less-illuminated slopes become more resistant to warming than slopes with more sunlight. It was beyond the scope of this study to address these possible feedbacks.

3. Domain characteristics

Central Colorado has characteristics that make it a favorable region for our simulations, including a large increase in terrain height and irregularity going westward from the plains up to the Continental Divide. Radiative heating and cooling of the sloping terrain drives a diurnal circulation that plays a large role in organizing summertime moist convection (Klitch et al. 1985; Toth and Johnson 1985). The dry climate and moderately high latitude are favorable for strong dependence of surface temperature on slope orientation. Simulations were made for conditions at the autumnal equinox, 23 September. Surface temperatures depend less on slope orientation near the summer solstice, when the sun's path is higher in the sky and sweeps through a broad range of azimuth angles. In the winter, surface thermal effects are strongly modulated by snow cover and synoptic disturbances.

The simulations were done for a 10′-wide band of terrain along 39°25′N, running from 104° to 107°W (Fig. 3). The numerical model grid was a vertical east–west cross section, with 19 horizontal grid points running along the center of the band at 10′ spacing and 26 levels in the vertical ranging from 10 to 13 500 m above ground level. This arrangement provided enough terrain data to cover a horizontal grid box around each grid point. The model included eight additional grid points on each end of the domain of interest to lessen the computational effects of the lateral boundaries.

The slope and aspect angles for each subgrid terrain element were computed from digital terrain-elevation data obtained at 3″ resolution from the Defense Mapping Agency (1977). The elevations of the model grid points were computed as simple averages over 10′ squares. Frequency distributions of subgrid slope angles illustrate that the terrain was much more irregular in the west than in the east (Fig. 4). For the vast majority of terrain elements the computed sunrises and sunsets occurred within 2 h of dawn or dusk, but at every hour of the day there were at least a few elements in shadow.

The simulation period ran from 0000 to 1800 local solar time (LST) using a 90-s time step and was preceded by a 3-h dynamic initialization. The daylight hours of 0600–1800 LST were the focus of satellite-related analysis. The surface and soil characteristics used in the model are listed in Table 1. The background (synoptic-scale) geostrophic wind was specified to be weak (1 m s^{-1} from the south), allowing thermally forced circulations to dominate. The initial potential temperature profile had a rate of 4 K km^{-1} from the ground to 9 km and 8 K km^{-1} above. The initial soil temperature profile was based on average late-September data from Fort Collins, Colorado, provided by the Colorado Climate Center. Initial values were set as differences from the air temperature at the lowest grid level.

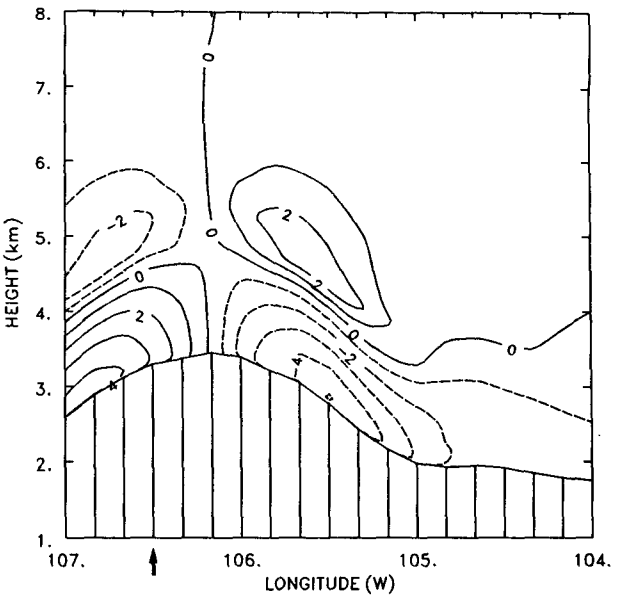

FIG. 3. The simulation domain, with westerly wind component (m s^{-1}) from the control model run at 1200 local time. Contour intervals are 1 m s^{-1}, with dashed lines for negative values (easterlies). Height is relative to sea level. Vertical hatching denotes the terrain, with the lines at model grid points. The arrow indicates the grid point referred to in Figs. 1, 5, and 7.

4. Results

a. Modeled surface temperatures

The model was first run in a control mode, in which there was no parameterization of subgrid surface temperature variations. Variations in the cooling and heating of the ground depended only on grid-resolved characteristics of the surface, the atmosphere, and the soil, including influences of elevation and slope orientation. Nocturnal cooling of the air along the mountainsides forced downslope near-surface flow through 0800 LST, with a reversal to upslope flow by midday in response to solar heating (Fig. 3). Gridded surface temperatures at 1200 LST ranged from 35°C over the plains to 26°C over the high mountains. This slope

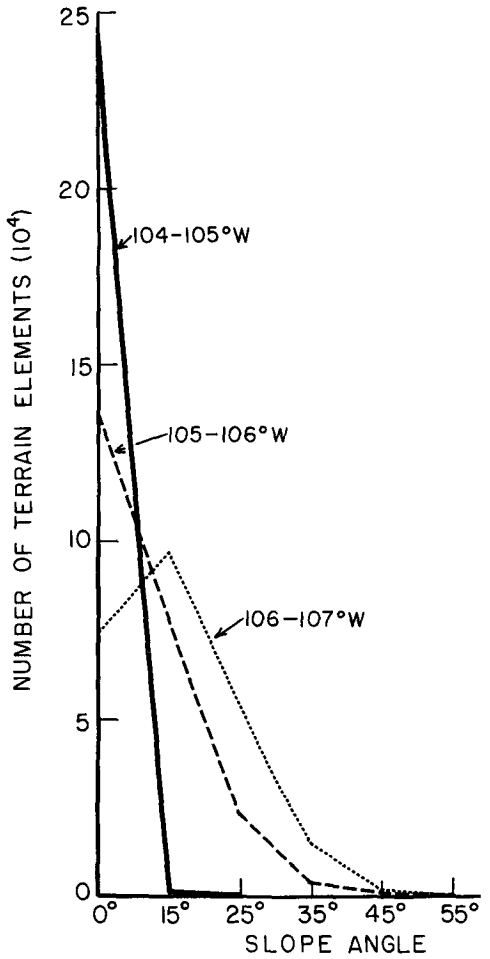

FIG. 4. Frequency of occurrence of terrain-element slope angles, regardless of aspect angle. Each curve represents the elements in one-third of the analysis domain, as identified by the curve labels.

flow regime was the meteorological setting for all of the experiments discussed below. A second model run included parameterization of 3″ terrain and resulted in grid-box average temperatures that were only about 1°C cooler in the mountains than the corresponding grid values in the control. These results are consistent with Avissar and Pielke's (1989) simulations of dry terrain with moderate slope angles.

The occurrence of biases in satellite-view temperatures depends on the variability of surface temperatures within small areas. The variability for a mountain grid box (106°30′W) is illustrated in Fig. 5, where temperatures ranged over 33°C at 0900 LST. From sunrise to 0900 LST the sun was low in the east-southeastern sky and, therefore, the warmest terrain elements at 0900 LST were the ones that faced east or southeast with slope angles of 35° or greater. The coolest elements were those that were still in shadow, including all elements that faced west-southwest at steep angles. The distribution of temperatures at 1500 LST was narrower than at 0900 LST, in part because a smaller proportion of the elements in the grid box were shaded (1% vs 4%). Another factor was that the shaded elements at 1500 LST had their temperatures moderated by heat that had been stored in the soil while they were illuminated earlier in the day. Nevertheless, there were substantial frequencies of temperatures over a 15°C range even at 1200 LST, when the sun was at its highest.

The data reported by Whiteman et al. (1989a,b) from Brush Creek Canyon in Colorado provided an opportunity to validate the surface temperatures computed by the model. In Table 2 are surface radiative temperature observations from sites on the southwest- and northeast-facing walls of the canyon on 25 September 1984 along with temperatures from the model. The elevation of the selected model grid point was about that of the observations and the model temperatures were interpolated from the slope–aspect classes that most nearly matched the slope–aspect angles of the canyon walls.

The agreement between the model results and the observations is generally close, despite the fact that the model was not initialized specifically for the meteorological conditions of the observation day and location. The time changes and the differences between the site temperatures were similar in the observations and the model, except for the northeast-facing site in the morning (see 0900 LST data). The discrepancy in that instance could have been due to a difference in shading histories, given that the northeast-facing site was shaded for the first hour of the morning, whereas the computations assumed no shading. Model computations were repeated for that site, with shading for the first hour, and indicated that the shading difference only accounted for 0.5°C of the discrepancy. The major part of the discrepancy appears to be due to the model's assumption of uniform, relatively dry soil. The observed volume fractions of water in the soil were 0.050 and 0.185 at the southwest- and northeast-facing sites, respectively. These moisture differences, along with differences in vegetation, led to large differences between the sites with respect to the use of solar energy for evaporating water versus heating the soil (Whiteman et al. 1989b). The model did not include aspect-dependent differences of this kind.

b. Effect of satellite viewing geometry

Satellite-view surface temperatures were computed from the parameterized model results as in Eq. (2),

TABLE 1. Soil and surface characteristics in the numerical model.

Soil wetness factor	0.04
Soil thermal conductivity	3.0×10^{-7} m^2 s^{-1}
Soil density	1.5×10^3 kg m^{-3}
Soil specific heat	1.25×10^3 J kg^{-1} K^{-1}
Surface roughness length	0.1 m
Surface albedo	0.2

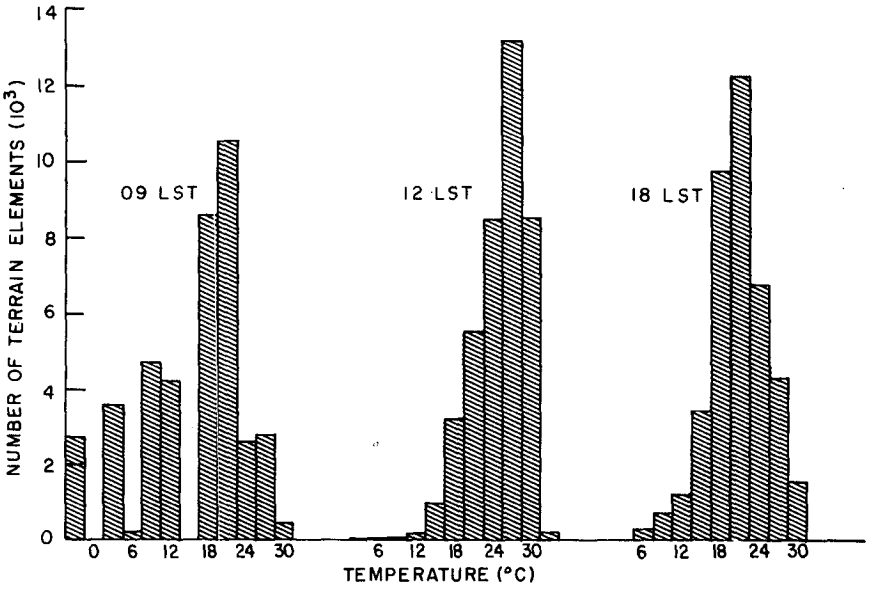

FIG. 5. Frequency of occurrence of surface temperatures among terrain elements in the grid box centered at 106°30′W (see Fig. 3). The plots correspond to the three local times given in the plot labels. Temperatures have been grouped within ranges of 3°C. The discontinuity of the frequency distribution is due to the assignment of elements to discrete slopes–aspect classes.

except that the terrain-element temperatures were averaged in groups according to class instead of individually. The averaging area was one grid box, which simulates a satellite sounding field of view of 14 × 19 km^2 and is comparable to a view from a VAS large detector (Menzel et al. 1983). Terrain elements that were obstructed from the satellite's view were omitted from the average, where obstruction was determined using the algorithm described in section 2. These satellite-view temperatures simulate what would be retrieved from error-free sounder data in an algorithm that perfectly accounts for atmospheric radiation and surface emittance variations and, therefore, isolates the view-dependent bias effect from all other potential sources of error. To quantify the bias, these satellite-view temperatures were compared with "true" average temperatures, which are simple averages of terrain-element temperatures over the same grid boxes.

The first viewing geometry considered was for a geostationary satellite at longitude 75°W, which was the data source in the Lipton and Vonder Haar (1990b) study. From the point of view of the study region, the satellite was toward the southeast, with a zenith angle ϕ of 55° and an azimuth (north-referenced) angle α of 137°. Differences between the geostationary-view temperatures and the true average temperatures were 3.2°C at most (Fig. 6). The largest differences occurred in the morning, when the sun was in the same part of the sky as the satellite and therefore the slopes viewed most directly by the satellite were the warmest ones. Conversely, the differences were small in the afternoon

TABLE 2. Surface temperatures (°C) for two sides of Brush Creek Canyon, Colorado.

Slope angle (deg)	Azimuth angle (deg)	Observations, Local time 0900	Observations, Local time 1200	Observations, Local time 1500	Model, Local time 0900	Model, Local time 1200	Model, Local time 1500
42	240	8	24	31	12	29	34
36	76	13	22	15	29	27	15

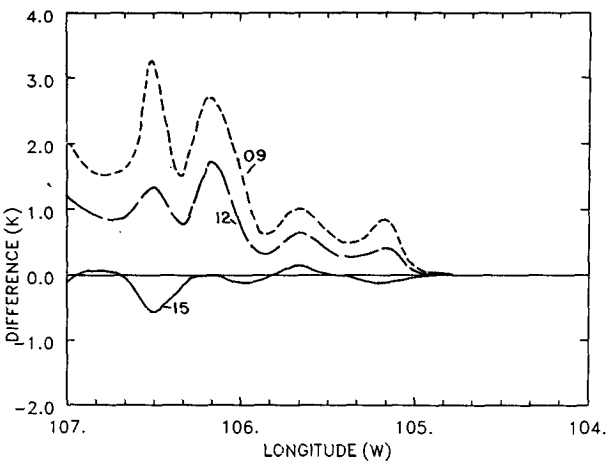

FIG. 6. Grid-average surface temperatures differences for the simulation domain: average weighted according to the view from a geostationary satellite at 75°W minus a simple average. The three curves are labeled according to local time.

due to the poor alignment of the sun's rays (from the southwest) with the satellite viewing angle. This trend is further illustrated in Fig. 7, where surface temperatures are plotted as a function of time for one grid box.

A satellite view corresponding to a look from the northwest by the High-Resolution Infrared Sounder (HIRS) was also considered, with $\phi = 55°$ and $\alpha = 290°$. This viewing geometry occurs when the NOAA satellite, on which the HIRS is mounted, is in the descending (equatorward) part of its orbit and the HIRS scanner is pointed toward the left. The temperature biases were of about the same magnitude as those for the geostationary view but were of opposite sign (Fig. 7). If HIRS retrievals for this region were compared with geostationary retrievals, there would be apparent discrepancies of up to 6.5°C if the view biases were not accounted for. The cross-track scanning method that the HIRS employs could also give rise to cross-track biases in retrieved temperature, given that the viewing azimuth changes by 180° as the HIRS scans across its nadir.

With a geostationary satellite located straight south of Colorado ($\phi = 46°$, $\alpha = 180°$), the biases were positive throughout the day in the mountain region but never greater than 1.5°C (not shown). The smaller maximum bias, as compared to the case with the satellite at 75°W, results from the smaller zenith angle and the narrower range of surface temperatures (Fig. 5) at the time of closest alignment between the satellite and the sun (1200 LST). These two factors were highlighted separately by considering two more satellite viewing angles.

The factor related to satellite zenith angle was emphasized by computing biases for a geostationary satellite at 60°W, with $\phi = 65°$ and $\alpha = 122°$. This satellite position gives a view from the southeast, as with the satellite at 75°W, but has a 10° larger zenith angle. The maximum bias was 50% greater than for the 75°W satellite, although retrievals are generally not done at zenith angles as large as 65°.

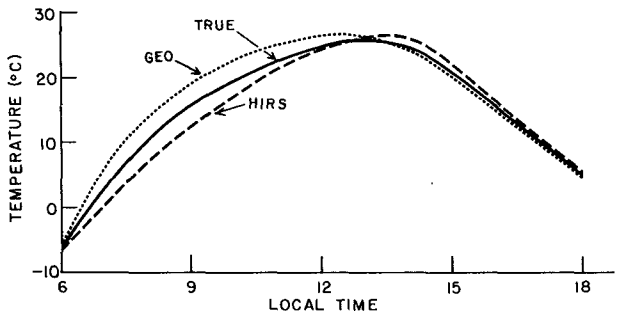

FIG. 7. Temperatures for the grid box centered at 106°30′W as a function of local time. The TRUE curve is a simple grid-box average, GEO is for a view from a geostationary satellite at 75°W, and HIRS is for a view from the HIRS sounder, as specified in the text.

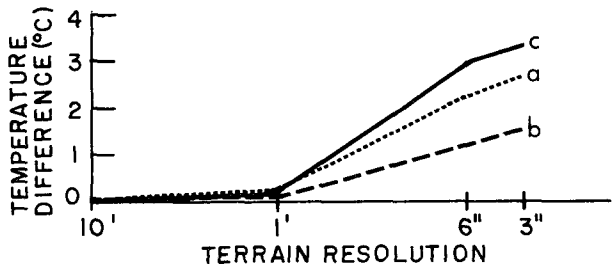

FIG. 8. Satellite-view temperature biases (satellite-view temperature minus simple grid-average temperature) for a geostationary satellite at 75°W as a function of the resolution of the terrain data used in the simulation. Biases are for grid points at (a) 106°10′W, (b) 106°20′W, and (c) 106°30′W at 0900 LST.

A satellite view from $\phi = 55°$ and $\alpha = 223°$ emphasized the impact on biases of narrowing the range of surface temperatures. This view from the southwest has the same zenith angle as for the geostationary satellite at 75°W, but is most closely aligned with the sun in the afternoon instead of in the morning. The maximum bias was less than for the satellite at 75°W—1.8°C versus 3.2°C—because the range of surface temperatures at 1500 LST was narrower than at 0900 LST (Fig. 5).

c. *Radiance averaging*

The above results excluded the effect of nonlinearity in the radiance–temperature relationship, given that Eq. (2) was used in the computations. The magnitude of the nonlinearity effect was explored by recomputing the results for the geostationary satellite at 75°W using Eq. (1), with $\epsilon_i = 1$, and then taking $T_s = B_\lambda^{-1}(L_s)$. The difference in results was only about 0.1°C for a sounder channel at 11 μm, but at 3.7 μm the results of using Eq. (1) were up to 0.7°C warmer than the results derived from Eq. (2). The nonlinearity effect is, therefore, of secondary importance in rugged terrain as compared to the effect of viewing geometry.

d. *Effect of terrain resolution*

Two additional simulations were performed to examine the effect of terrain data resolution on the computed satellite-view temperature biases. The simulation methods were the same as with 3″ data, but were applied to terrain data averaged to resolutions of 6″ and 1′. Satellite-view temperatures were computed for a geostationary satellite at 75°W. Biases for three mountain grid points at 0900 LST are given in Fig. 8 as a function of subgrid terrain resolution. The lower-resolution datasets had fewer steep slopes and, therefore, smaller computed biases. Biases were zero for 10′ resolution (the control) because a single terrain element covered the entire satellite field of view, and virtually no bias was resolved for 1′ data.

The curves in Fig. 8 imply that 3″ data are of insufficient resolution to show the full potential magnitude of satellite-view biases, given that the biases were still increasing functions of finer resolution at the 3″ point. At some resolution the curves must level off. There may be a scale at which finer-resolution data no longer corresponds to a larger proportion of steep slopes and, ultimately, a scale at which temperature contrasts between adjacent slopes are damped by horizontal heat conduction in the soil. Nevertheless, slope-dependent surface temperature variations have been observed at scales as small as agricultural furrows (Geiger 1965, p. 388) and, thus, it is likely that true satellite-view biases would be substantially larger than those represented by 3″ data. The 3″ results can be thought of as a lower limit on the view-dependent biases, subject to the many assumptions and approximations inherent in the simulation method. An absolute upper limit on the biases (at 0900 LST) is about 19°C, which is the bias value that would occur if the subresolution terrain consisted entirely of steep, parallel ridges with sides facing southeast and northwest.

e. Sensitivity of modeled winds

An experiment was conducted to show the effect of using view-biased data to specify surface temperatures in mesoscale modeling of the Colorado domain. The model was run using gridded surface temperatures taken from the earlier 3″ parameterized simulation, but with biases added from the computations for a geostationary satellite at 75°W. Given that the biases had been computed at 3-h intervals, the temperatures for each model time step were interpolated using cubic splines fit to 3-h–biased temperatures. For comparison, another model run was made with splines fit to unbiased temperatures, yielding winds very similar to those in Fig. 3.

The bias-induced differences in modeled winds (not shown) were small in comparison to the upslope–downslope circulation of the control. Westerly wind component differences were no more than 0.5 m s^{-1} in the low-level upslope region, and vertical velocity differences were up to 3 cm s^{-1}. These differences correspond to about 10% and 20%, respectively, of the strength of the control circulation.

These wind differences are specific to the domain and synoptic situation of the simulation. The relative effect of biases might have been less if, for example, there was a synoptic disturbance affecting the domain. These results indicate that the effect of view-dependent biases on satellite data assimilation is small in relation to the locally forced circulations.

f. Domain dependence

The bias magnitudes presented above are particular to the distribution of slope orientations in central Colorado, where slopes steeper than 15° are unusual and slopes steeper than 25° are rare (Fig. 4). Other mountain ranges; such as the Sierra Nevada, the Andes, and the Himalayas; may include regions with substantially rougher terrain than the study domain. The potential for greater satellite-view biases than those presented above was investigated by considering idealized terrain. Biases were computed for terrain consisting of equal areas of north- and south-facing slopes of equal steepness, as viewed from the south with a satellite zenith angle of 50°. Computations were also made for a mixture of east- and west-facing slopes viewed from the east. Surface temperature data for the computations were taken from the grid box at 106°30′W in the model run with 3″ subgrid terrain. The biases (Fig. 9) were strongly dependent on the steepness of the slopes, particularly for slope angles greater than 25°.

5. Conclusion

The simulations reported here indicate that local variations in slope orientation can lead to surface temperature variations up to 30°C for autumn conditions in the mountains of Colorado. For realistic satellite viewing conditions, these variations can give rise to biases in retrieved surface temperatures of about 3°C,

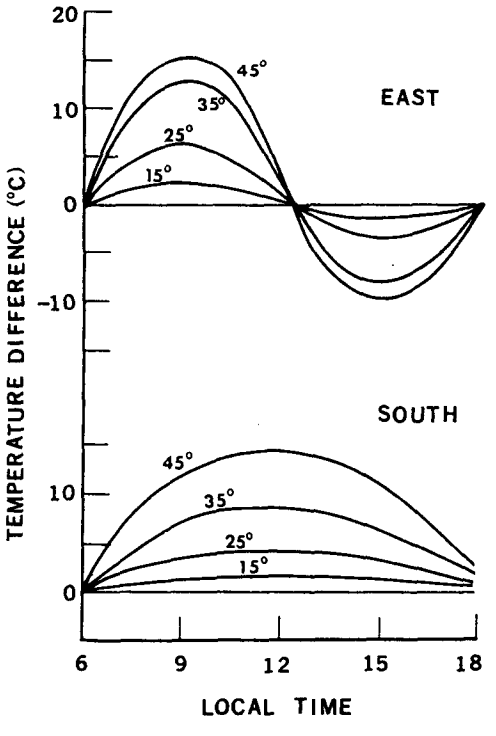

FIG. 9. Satellite-view temperature biases as a function of local time for equal areas of east- and west-facing slopes as viewed from the east (top) and north- and south-facing slopes as viewed from the south (bottom). The curves are labeled according to the slope angles. The satellite zenith angles are 50° for both views.

due to the correlations between the slopes' temperatures and their orientations with respect to the satellite. This bias effect can therefore be at least as large as the effect of varying surface emittances. Relative biases between retrievals from two satellites can be over 6°C, which could lead to confusion when merging datasets. The bias computations were limited by the resolution of the available terrain height data (~90 m), and the results suggest that the biases would be significantly larger if the data resolution was fine enough to represent every detail of the Colorado terrain. Biases could also be much larger in mountain areas that have a larger proportion of steep slopes than the Colorado Rockies. On the other hand, observational data indicate that there would be no detectable biases in areas with dense vegetation and high evapotranspiration (Sader 1986).

Simulations in which surface temperature retrievals with view-dependent biases were assimilated into time-continuous analyses indicated that the bias gradients across the Colorado domain were not large enough to significantly alter the forcing of the diurnal upslope–downslope circulations. However, we cannot conclude that view-dependent biases are of negligible importance to mesoscale assimilation, given the limited resolution of the terrain elevation data used in the computations.

One could compensate for view-dependent biases in satellite–model coupled mesoscale analysis methods if the model includes a parameterization of subgrid surface temperatures. In the current Lipton and Vonder Haar (1990a) analysis method, model surface temperatures are adjusted according to the differences between the retrieved temperatures and the initial guess temperatures, where the initial guesses are taken from model data. The method could be altered so that the initial guesses are based on subgrid temperatures weighted according to the satellite viewing angle, as in Eq. (2). There would then be no view-dependent biases in the retrieval–initial guess differences and, hence, no biases would be introduced when the model surface temperatures are adjusted.

View-dependent retrieval biases may be relevant to climatological research, given the increasing reliance on remotely sensed data for climate monitoring. Bias-induced errors are systematic and, thus, can interfere with analysis of temporal and spatial variations of surface characteristics, even when the analysis is based on averages of many observations.

A significant drawback to compensating for the view-dependence of retrievals is the cost in computer time and storage space. The small region dealt with in this study included 1.44×10^6 terrain elements, and the shading computations required nearly 9 h of CPU time on a VAX 6000. A mitigating factor is that the shading and classification computations do not need to be repeated for every analysis, given that their results change only with season. The model integration time was approximately doubled when the parameterization of subgrid temperatures was invoked, although the increase could be reduced by using fewer slope orientation classes.

Acknowledgments. The author thanks Dr. C. D. Whiteman for graciously providing information useful for developing and validating the numerical model. T. Kleespies and J. W. Snow are thanked for thoughtfully reviewing the original manuscript, O. Bliss and N. Doesken for providing Colorado climate data, C. Wiley for help with literature searches, and B. Main for drafting figures.

APPENDIX

Diffuse Radiation

The radiation parameterization of the model was modified to distinguish between shaded terrain elements, which receive only diffuse solar radiation, and directly sunlit elements. The modified method assumed, however, that each element was fully exposed to the sky, so computations of incoming radiation did not account for solar reflection or infrared emission from neighboring terrain elements.

The model (Mahrer and Pielke 1977) computes the total (direct and diffuse) radiation on an inclined surface as

$$R_T = S_0 \cos\eta(1 - A)(\tau_T - a_W), \qquad \text{(A1)}$$

where S_0 is the solar radiation at the top of the atmosphere, η is the solar incidence angle on a sloping surface, A is surface albedo, a_W is absorption due to water vapor, and τ_T is the transmittance that accounts for Rayleigh scattering and absorption by all gases except water vapor. The transmittance function is a modification (Atwater and Brown 1974) of Kastrov's function τ_0 (Kondratyev 1969) such that

$$\tau_T = 0.485 + 0.515\tau_0, \qquad \text{(A2)}$$

where τ_0 neglects *forward* Rayleigh scattering and thus represents direct radiation. For our simulations, the diffuse radiation was computed from the difference between these two transmittances such that

$$R_D = S_0 \cos\zeta(1 - A)(\tau_T - \tau_0), \qquad \text{(A3)}$$

where ζ is the solar zenith angle. This method gives an adequate estimate of the diffuse radiation without requiring major changes to the model formulation. Results of the method were compared with the observations of Whiteman et al. (1989a). Computed values of diffuse irradiance tended to be lower than observed values, with differences of 45 W m^{-2} being the worst.

REFERENCES

Astling, E. G., and D. A. Quattrochi, 1989: Thermal characteristics of mountain desert terrain derived from thermal infrared multispectral scanner measurements. Tech. Papers, ASPRS/ACSM Annual Meeting, Baltimore, 3, 217–225. [AIAA A90-46434.]

Atwater, M. A., and P. S. Brown Jr., 1974: Numerical computations

of the latitudinal variation of solar radiation for an atmosphere of varying opacity. *J. Appl. Meteor.*, **13,** 289–297.

Avissar, R., and R. A. Pielke, 1989: A parameterization of heterogeneous land surfaces for atmospheric numerical models and its impact on regional meteorology. *Mon. Wea. Rev.*, **117,** 2113–2136.

Blackwell, D. D., J. L. Steele, and C. A. Brott, 1980: The terrain effect on terrestrial heat flow. *J. Geophys. Res.*, **85,** 4757–4772.

Defense Mapping Agency, 1977: Product specifications for Digital Landmass System (DLMS) data base, 126 pp. [Available from Director, DMA Aerospace Center, 3200 S Second St, St. Louis, MO 63118-3300.]

Geiger, R., 1965: *The Climate near the Ground.* Harvard University Press, 611 pp.

Klitch, M. A., J. F. Weaver, F. P. Kelly, and T. H. Vonder Haar, 1985: Convective cloud climatologies constructed from satellite imagery. *Mon. Wea. Rev.*, **113,** 326–337.

Kondratyev, K. Ya., 1969: *Radiation in the Atmosphere.* Academic Press, 912 pp.

Kornfield, J., and J. Susskind, 1977: On the effect of surface emissivity on temperature retrievals. *Mon. Wea. Rev.*, **105,** 1605–1608.

Lipton, A. E., and T. H. Vonder Haar, 1990a: Mesoscale analysis by numerical modeling coupled with sounding retrieval from satellites. *Mon. Wea. Rev.*, **118,** 1308–1329.

——, and ——, 1990b: Preconvective mesoscale analysis over irregular terrain with a satellite/model coupled system. *Mon. Wea. Rev.*, **118,** 1330–1358.

Mahrer, Y., and R. A. Pielke, 1977: A numerical study of the air flow over irregular terrain. *Con. Atmos. Phy.*, **50,** 98–113.

——, and ——, 1978: A test of an upstream spline interpolation technique for the advective terms in a numerical mesoscale model. *Mon. Wea. Rev.*, **106,** 818–830.

McNider, R. T., and R. A. Pielke, 1981: Diurnal boundary layer development over sloping terrain. *J. Atmos. Sci.*, **38,** 2198–2212.

Menzel, W. P., W. L. Smith, G. S. Wade, L. D. Herman, and C. M. Hayden, 1983: Atmospheric sounding from a geostationary satellite. *Appl. Opt.*, **22,** 2686–2689.

Sader, S. A., 1986: Analysis of effective radiant temperatures in a Pacific Northwest forest using thermal infrared multispectral scanner data. *Rem. Sens. Envir.*, **19,** 105–115.

Sutherland, R. A., 1986: Broadband and spectral emissivities (2–18 μm) of some natural soils and vegetation. *J. Atmos. Ocean. Tech.*, **3,** 199–202.

Toth, J. J., and R. H. Johnson, 1985: Summer surface flow characteristics over northeast Colorado. *Mon. Wea. Rev.*, **113,** 1458–1469.

Van de Griend, A. A., M. Owe, M. Groen, and M. P. Stoll, 1991: Measurement and spatial variation of thermal infrared surface emissivity in a savanna environment. *Water Resour. Res.*, **27,** 371–379.

Whiteman, C. D., K. J. Allwine, L. J. Fritschen, M. M. Orgill, and J. R. Simpson, 1989a: Deep valley radiation and surface energy budget microclimates. Part I: Radiation. *J. Appl. Meteor.*, **28,** 414–426.

——, ——, ——, ——, and ——, 1989b: Deep valley radiation and surface energy budget microclimates. Part II: Energy budget. *J. Appl. Meteor.*, **28,** 427–437.